A chemiresistive methane sensor

Máté J. Bezdek[a], Shao-Xiong Lennon Luo[a], Kang Hee Ku[a], and Timothy M. Swager[a,1]

[a]Department of Chemistry and Institute for Soldier Nanotechnologies, Massachusetts Institute of Technology, Cambridge, MA 02139

Contributed by Timothy M. Swager, December 1, 2020 (sent for review October 28, 2020; reviewed by Cathleen Crudden and Colin Nuckolls)

A chemiresistive sensor is described for the detection of methane (CH_4), a potent greenhouse gas that also poses an explosion hazard in air. The chemiresistor allows for the low-power, low-cost, and distributed sensing of CH_4 at room temperature in air with environmental implications for gas leak detection in homes, production facilities, and pipelines. Specifically, the chemiresistors are based on single-walled carbon nanotubes (SWCNTs) noncovalently functionalized with poly(4-vinylpyridine) (P4VP) that enables the incorporation of a platinum-polyoxometalate (Pt-POM) CH_4 oxidation precatalyst into the sensor by P4VP coordination. The resulting SWCNT-P4VP-Pt-POM composite showed ppm-level sensitivity to CH_4 and good stability to air as well as time, wherein the generation of a high-valent platinum intermediate during CH_4 oxidation is proposed as the origin of the observed chemiresistive response. The chemiresistor was found to exhibit selectivity for CH_4 over heavier hydrocarbons such as *n*-hexane, benzene, toluene, and *o*-xylene, as well as gases, including carbon dioxide and hydrogen. The utility of the sensor in detecting CH_4 using a simple handheld multimeter was also demonstrated.

methane | sensor | chemiresistors | selectors | catalysis

The selective detection of methane (CH_4) is paramount to environmental health as well as human safety in both domestic and industrial settings. On one hand, CH_4 is a high-impact anthropogenic greenhouse gas with a global warming potential 86 times larger than that of carbon dioxide (CO_2) over a 20-y period (1). Colorless and odorless, methane also poses an acute explosion hazard at a concentration range of approximately 5 to 15% in air, an omnipresent risk in distribution centers, mines, and petroleum fractional distillation plants (2).

While environmental CH_4 levels are typically monitored using gas chromatography (3) and optical gas analyzers (4–6), the development of alternative materials and approaches for CH_4 detection is ongoing (7–9) and includes pellistors (10, 11), metal oxides (12–14), photoacoustic devices (15), as well as electrochemical (16, 17) and thermal wave sensors (18). Although high sensitivities can be achieved using some of these methods, drawbacks typically include poor selectivity, high device power consumption, elevated operational temperatures, as well as expensive and bulky device enclosures that are impractical for real-time, high-spatial-resolution field measurements. As a result, new CH_4 sensing technologies are needed that are compact, inexpensive, and portable with operational capability at or near ambient conditions.

Chemiresistors sensitive to analyte interactions offer a potential solution to these challenges (19). In particular, single-walled carbon nanotubes (SWCNTs) are an attractive chemiresistor class owing to inexpensive fabrication, room-temperature operation, as well as ultra-low power requirements (20, 21). Pristine (unfunctionalized) SWCNTs show no response to methane at room temperature and, as a result, introduction of a selector is necessary to translate a molecular interaction into an electrical signal. Methane sensing using SWCNTs is still at an early stage, however, owing to the difficulty of obtaining a selective response to the nonpolar and inert CH_4 molecule via traditional selector–analyte interaction strategies such as adsorption (22, 23), swelling (24, 25), receptor/guest interactions (26–28), or chemical reaction (29). For example, Star et al. constructed gas sensor arrays using metal-decorated SWCNTs but found no significant response to CH_4 in the composites featuring 18 different metals (30). Previously, conductance changes were reported for both SWCNTs and multiwalled CNTs decorated with Pd (31) and SnO_2/ZnO nanocrystals (32, 33), respectively, upon exposure to CH_4. However, in addition to cumbersome sensor preparation, cross-reactivity studies with other gases were not carried out and the mechanistic origins of the observed conductance changes remain unclear, hampering rational sensor development using such nonmolecular systems. Therefore, fundamentally new approaches are needed for designing metal-CNT composites that can be readily fabricated, exhibit long-term stability, sensitivity, and selectivity toward CH_4 such that the distributed, low-power, and low-cost sensing of CH_4 may be realized.

An emerging strategy for analyte detection using SWCNTs involves a room-temperature chemical reaction of the analyte catalyzed by a selector on the SWCNT surface (34, 35). This approach is particularly attractive because the selector is not consumed during analyte detection, thus enabling long-term device stability and dose-independent sensitivity. Because SWCNT charge carrier densities are sensitive to surface electronic changes and can be modulated by catalyst redox cycling, the chemoselectivity of the surface reaction may be translated to selective analyte detection (34, 35). Herein we report the application of this concept to the detection of CH_4 under ambient conditions. Specifically, we incorporate a platinum-polyoxometalate (Pt-POM) aerobic CH_4 oxidation precatalyst reported by Bar-Nahum et al. (36) and Villalobos et al. (37) into a SWCNT-based chemiresistor, with the goal of translating the redox cycling of the catalyst during CH_4 oxidation to a chemiresistive response (Fig. 1). This particular catalytic system was targeted due to its unique reported activity in aqueous aerobic CH_4 oxidation under mild conditions,

Significance

Methane is potentially explosive and is a major threat to environmental health as a potent greenhouse gas. However, its volatility and nonpolar nature render selective methane detection a significant challenge. Here we report a chemiresistive sensor based on single-walled carbon nanotubes and a molecular platinum-polyoxometalate complex known to mediate methane oxidation near ambient conditions. We show that the composite is a robust sensor that operates at room temperature, exhibits air and moisture stability, as well as selectivity for methane. Our results demonstrate that concepts in molecular methane oxidation can be leveraged to develop low-power, low-cost, and potentially distributable sensors for selective methane detection.

Author contributions: M.J.B. and T.M.S. designed research; M.J.B., S.-X.L.L., and K.H.K. performed research; M.J.B., S.-X.L.L., K.H.K., and T.M.S. analyzed data; and M.J.B. and T.M.S. wrote the paper.

Reviewers: C.C., Queen's University, Canada; and C.N., Columbia University.

Competing interest statement: A patent has been filed on this technology.

[1]To whom correspondence may be addressed. Email: tswager@mit.edu.

This article contains supporting information online at https://www.pnas.org/lookup/suppl/doi:10.1073/pnas.2022515118/-/DCSupplemental.

Published December 31, 2020.

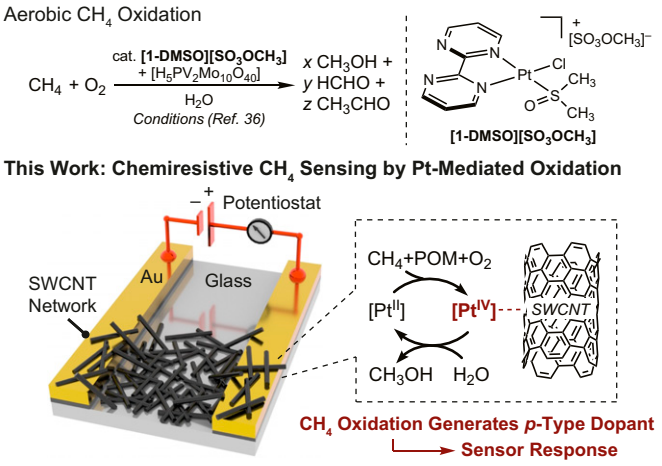

Fig. 1. Aerobic methane oxidation with a platinum-polyoxometalate precatalyst under mild conditions and the strategy reported in the present study. SWCNT, single-walled carbon nanotube; POM, polyoxometalate [$H_5PV_2Mo_{10}O_{40}$].

enabled by the use of a POM cocatalyst ($H_5PV_2Mo_{10}O_{40}$) that was proposed to mediate the key Pt(II)-Pt(IV) oxidation while itself being regenerated by O_2 (36). By repurposing the robust Pt-POM precatalyst system as a selector, we obtain a lightweight chemiresistor for the selective detection of CH_4 at room temperature in air, presenting a viable technology for the in-field, real-time monitoring of this challenging analyte.

Results and Discussion

Fabrication and Characterization of Chemiresistors. Our studies commenced with the fabrication of a SWCNT-based film incorporating the Pt-POM precatalyst in Fig. 1 for use as a chemiresistor. First, SWCNTs were dispersed in a dimethylformamide solution containing P4VP [P4VP = poly(4-vinylpyridine); SWCNT:P4VP 1:10 wt/wt] and spray coated between gold electrodes on glass at 140 °C (1-mm gap, chromium adhesive layer) in a four-channel array with a shared counter electrode (Fig. 2*A*, step 1). P4VP serves to debundle SWCNTs through pyridyl lone pair-π and π-π interactions with the CNT sidewalls (38), thereby increasing the analyte-accessible SWCNT surface area while restricting nanotube conduction pathways, attributes that are expected to yield improved chemiresistive-sensing properties. In addition, free pyridyl groups in P4VP can be utilized to introduce metal selectors into the SWCNT-P4VP matrix by coordination (39). Accordingly, the device bearing the SWCNT-P4VP film was soaked in a DMSO solution containing [(bpym)Pt(DMSO)Cl][SO_3OCH_3] ([1-DMSO][SO_3OCH_3]; bpym = 2,2′-bipyrimidine, DMSO = dimethyl sulfoxide) for 18 h at room temperature in order to immobilize the Pt complex in the SWCNT-P4VP network (SWCNT-P4VP-Pt; Fig. 2*A*, step 2). The device was subsequently soaked in a DMSO solution of the POM [$H_5PV_2Mo_{10}O_{40}$] for 18 h at room temperature in order to achieve anion exchange, thus furnishing the targeted SWCNT-P4VP-Pt-POM composite (Fig. 2*A*, step 3). The speciation of the Pt-POM complex on the chemiresistor surface (Fig. 2 *B* and *C*) is discussed in greater detail below.

The composites SWCNT-P4VP, SWCNT-P4VP-Pt and SWCNT-P4VP-Pt-POM were characterized by Fourier transform infrared (FTIR) spectroscopy in order to probe surface immobilization chemistry and subsequent anion exchange (*SI Appendix*, Fig. S4). The FTIR spectrum of a SWCNT-P4VP film exhibits diagnostic bands at 1,597 and 1,417 cm^{-1} corresponding to free pyridyl ring vibrations. In SWCNT-P4VP-Pt, metal coordination was evidenced by the shifting of these bands to 1,587 and 1,413, respectively, while a new vibration was observed at 1,220 cm^{-1}, attributed to the $[SO_3OCH_3]^-$ anion (40). Upon treatment with [$H_5PV_2Mo_{10}O_{40}$], anion exchange in the SWCNT-P4VP-Pt-POM composite was confirmed by the disappearance of the band at 1,220 cm^{-1} while new bands appeared at 945 and 785 cm^{-1} that correspond to the POM anion.

Metal incorporation as well as anion exchange in SWCNT-P4VP-Pt-POM was further probed by X-ray photoelectron spectroscopy (XPS; *SI Appendix*, Fig. S5). Diagnostic peaks corresponding to Pt $4f_{5/2}$ and Pt $4f_{7/2}$ binding energies were observed at 76.8 and 73.4 eV, respectively, supporting the incorporation of Pt(II) into the composite. Further, a high-resolution N 1s scan revealed a broad peak at 400.5 eV in SWCNT-P4VP-Pt, indicating that the majority of nitrogen atoms in both P4VP as well as the bpym ligand exist in a coordinated, rather than free form upon addition of the Pt complex to SWCNT-P4VP (41). Finally, a marked decrease in peak intensity was observed for the S 2p binding energy (167.8 eV) in SWCNT-P4VP-Pt-POM compared to SWCNT-P4VP-Pt, while new peaks were observed that correspond to P 2p, V $2p_{1/2}$, V $2p_{3/2}$, Mo $3d_{3/2}$, and Mo $3d_{5/2}$ binding energies at 132.8, 523.5, 516.0, 235.3, and 232.1 eV in SWCNT-P4VP-Pt-POM, respectively. Taken together, these XPS results confirm anion exchange and POM incorporation into the SWCNT-P4VP-Pt-POM composite.

To probe whether the incorporation of Pt-POM disrupts the π-electronic states in the SWCNT network by nanotube wall modification, SWCNT-P4VP, SWCNT-P4VP-Pt and SWCNT-P4VP-Pt-POM films were also characterized by Raman spectroscopy (532-nm excitation; *SI Appendix*, Fig. S6). In particular, the D/G band ratio was of interest in each composite, wherein nanotube sidewall defects give rise to an increased D band. Importantly, the D/G peak area ratios in SWCNT-P4VP, SWCNT-P4VP-Pt, and SWCNT-P4VP-Pt-POM were virtually unchanged (I_D/I_G = 0.09), indicating that the Pt-POM incorporation steps do not significantly affect the electronic structure of the SWCNTs.

Sensing Performance of Chemiresistors. Having established the composition of SWCNT-P4VP-Pt-POM, the utility of the composite as a chemiresistor in CH_4 sensing was examined. Our proof-of-concept sensing experiments were conducted in a gas-tight enclosure wherein two mass-flow controllers (MFCs) were utilized to deliver a mixture of CH_4 in air (RH = 10 ± 5%) at a flow rate of 1 L/min to the device (see *SI Appendix*, Fig. S3 for sensing schematic). The sensor signal was taken as the normalized change in device conductance [$\Delta G/G_0$ (%) = $(I–I_0)/I_0 \times 100\%$; I_0 = initial current] upon application of a voltage between the electrodes. Exposing the device to 0.5% (5,000 ppm) of CH_4 for 120 s at room temperature resulted in a significant sensor response corresponding to a 0.87 ± 0.16% increase in device conductance. The sensor response was found to be reversible, wherein nearly full baseline recovery was observed after purging for 120 s with air (Fig. 3 *A*, *Inset*). Importantly, a detrimental effect on sensor response was observed when each component of the SWCNT-P4VP-Pt-POM composite was omitted (Fig. 3*A*). For instance, a device fabricated with exclusion of P4VP yielded a negligible sensor response on the order of that observed for pristine SWCNTs, confirming that the pyridyl moiety is essential for anchoring the selector on the SWCNT surface. Further, while exclusion of the Pt cation resulted in a near-negligible sensor response, a device fabricated with the exclusion of POM (SWCNT-P4VP-Pt) showed a low-magnitude inverted response corresponding to a decrease in device conductance (−0.28 ± 0.03%), likely due to a change in sensing mechanism. Overall, these experiments establish that P4VP, Pt cation, and the POM anion are all key for the observed chemiresistive CH_4 sensing using SWCNT-P4VP-Pt-POM. Repeatedly exposing the sensor to 0.5% of CH_4 while purging with air between CH_4 doses resulted in reversible responses of consistent magnitude, indicating chemiresistor stability (Fig. 3*B*). Exposure of

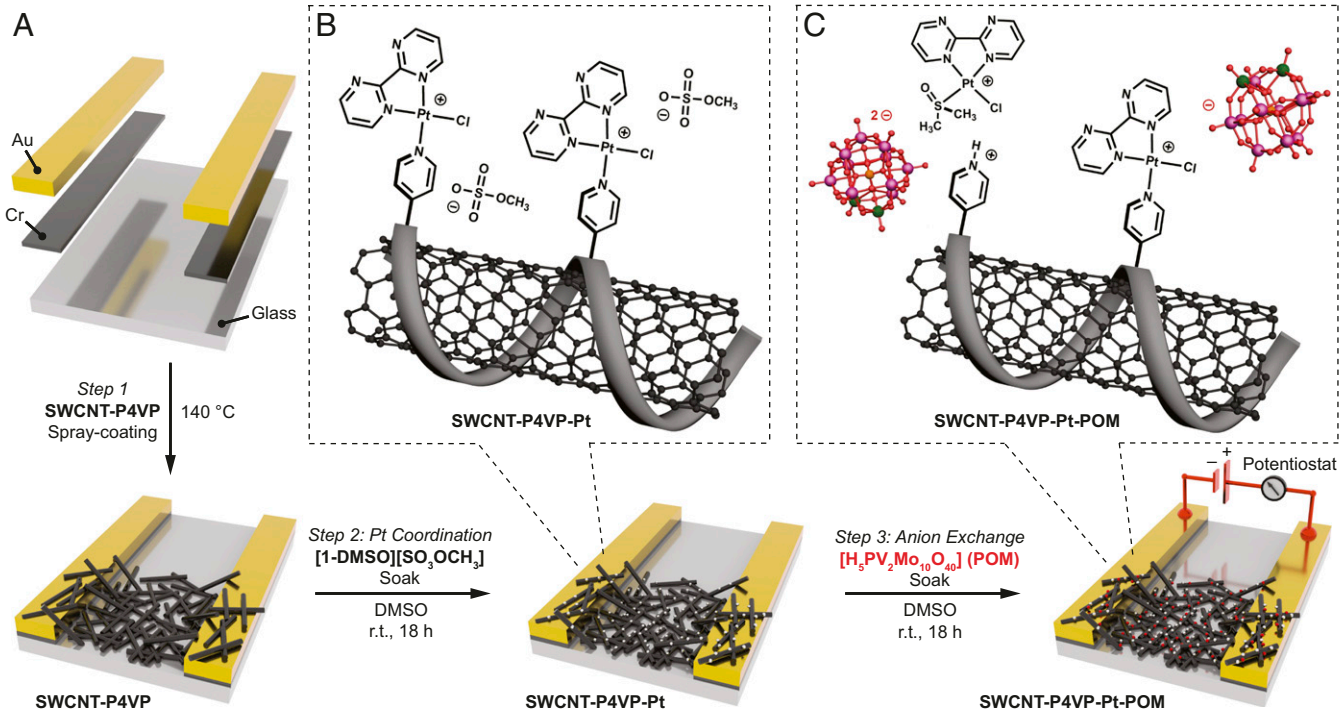

Fig. 2. Device fabrication schematic and chemiresistor composition. (*A*) Sensor fabrication and stepwise selector incorporation by spray coating of SWCNT-P4VP network (step 1), Pt coordination by soaking in [1-DMSO][SO_3OCH_3] solution (step 2), and anion exchange by soaking in [$H_5PV_2Mo_{10}O_{40}$] solution (step 3). (*B*) Proposed surface speciation of SWCNT-P4VP-Pt. (*C*) Proposed surface speciation of SWCNT-P4VP-Pt-POM.

the sensor to varying CH_4 concentrations yielded a linear change in response in the range of 50 to 1000 ppm (Fig. 3*C*), wherein the theoretical limit of detection (LOD) (42) for 120 s of exposure was calculated to be 29 ppm (Fig. 3*D*).

The reversible increase in device conductance observed when SWCNT-P4VP-Pt-POM was exposed to CH_4 is consistent with our working hypothesis that CH_4 oxidation should give rise to a signal. If a Shilov-type methane oxidation mechanism is operative, some platinum centers will transiently exist in a formal Pt(IV) state upon oxidation by the POM, wherein O_2 serves as the terminal oxidant that regenerates the POM (36, 43, 44). Given that SWCNTs are known to undergo *p*-type doping upon exposure to O_2 in air (45, 46), interactions with the high-valent, electron-deficient platinum metal centers will likely increase hole carrier density and thereby proportionally increase conductance. Consistent with an oxidation event in SWCNT-P4VP-Pt-POM is the observation that use of dinitrogen in place of air as the analyte carrier gas significantly attenuated the magnitude of the observed response but maintained its direction ($\Delta G/G_0 = 0.35 \pm 0.03\%$; 5,000 ppm CH_4, 120-s exposure; Fig. 3*C*). In this case, the POM likely serves as a less efficient, stoichiometric oxidant that is not regenerated by excess O_2 and likely accounts for the attenuated CH_4 response under anaerobic conditions. In addition, we observe that the device response in air deviates from linearity relative to [CH_4] in the range 2,500 to 5,000 ppm, likely due to an increased efficiency of CH_4 oxidation at the chemiresistor surface in the presence of larger amounts of the analyte (*SI Appendix*, Fig. S10).

The presence of humidity was also found to be key for optimal sensor performance as indicated by a lower response to CH_4 when dry air (RH = 0%) was used as the carrier gas ($\Delta G/G_0 = 0.58 \pm 0.08\%$; 5,000 ppm CH_4, 120-s exposure; Fig. 3*C*). We attribute the humidity effect to the proposed role of POM as an oxidant in enabling the key Pt(II)/(IV) oxidation (36, 47, 48). In this context, it is important to note that [$H_5PV_2Mo_{10}O_{40}$] is a hydrate in the solid state, containing 32 water equivalents/mol (49), wherein dehydration by exposure to vacuum results in a noticeable color change of the compound from orange to yellow-brown (*SI Appendix*, Fig. S9*A*). Dehydration in dry air therefore likely leads to a structural change that diminishes POM effectiveness as an oxidant during CH_4 sensing. Consistent with this qualitative observation, exposure of SWCNT-P4VP-Pt-POM to vacuum (approximately 1×10^{-3} mbar) for 5 h resulted in a dramatically lowered CH_4 response of $\Delta G/G_0 = 0.09 \pm 0.01\%$ (5,000 ppm CH_4, 120-s exposure; *SI Appendix*, Fig. S9*B*). Interestingly, submerging the device in water and subsequent evaluation of its sensing performance resulted in partial recovery of the signal to $\Delta G/G_0 = 0.43 \pm 0.03\%$ (*SI Appendix*, Fig. S9*B*). This result implies that the POM dehydration process is partially reversible and that contact with water is likely necessary to preserve the structural integrity of the POM selector and by extension, maintain sensor performance. Overall, these results are consistent with a CH_4 oxidation event by establishing the roles of O_2, H_2O, and POM structure during sensing.

Model Studies on Selector Speciation. We next sought to understand Pt speciation in the sensor composite in order to further support our working hypothesis invoking a Pt-mediated CH_4 oxidation. To this end, a ^{1}H NMR study was performed with soluble Pt complexes and pyridine as a model for P4VP. Stirring a DMSO-d_6 solution of [1-DMSO][SO_3OCH_3] in the presence of one equivalent of pyridine at room temperature for 18 h resulted in quantitative substitution of the DMSO ligand to afford the pyridine adduct [1-Py][SO_3OCH_3] (Fig. 4). The ^{1}H NMR spectrum (DMSO-d_6) of [1-Py][SO_3OCH_3] exhibits the number of resonances indicative of an overall C_s molecular symmetry, with pyridine resonances observed at 8.92, 8.27, and 7.82 ppm, consistent with coordination to the platinum center. Also indicative of DMSO ligand substitution was the lack of a diagnostic DMSO vibration in the IR spectrum of [1-Py][SO_3OCH_3] ($\nu_{S=O}$ = 1,128 cm^{-1} in [1-DMSO][SO_3OCH_3]). These data demonstrate

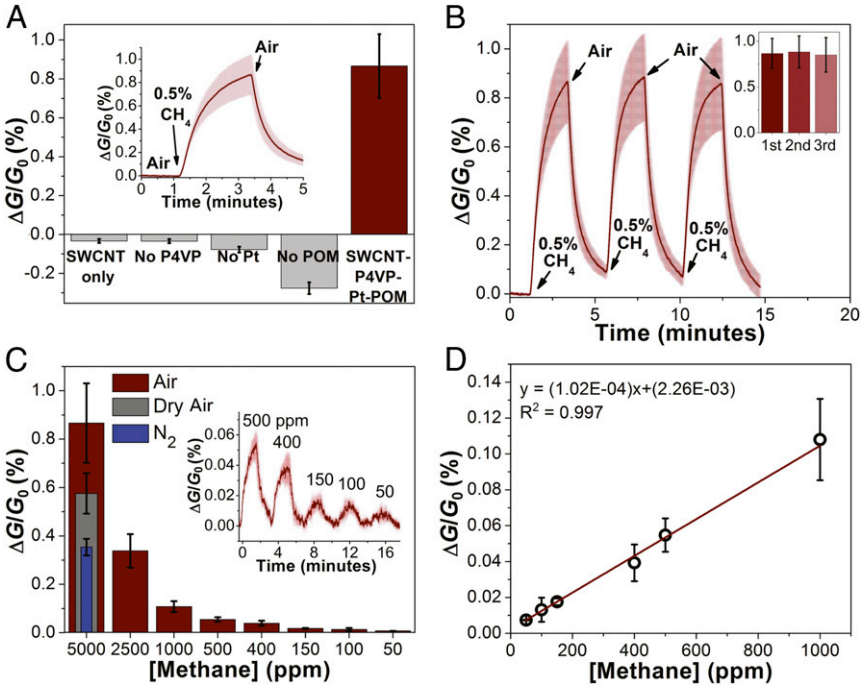

Fig. 3. Chemiresistor performance in methane sensing and control experiments. (*A*) Control CH_4 sensing experiments omitting selector components contrasted with the sensing response of SWCNT-P4VP-Pt-POM. (*Inset*) Averaged change in conductance (represented as $\Delta G/G_0$, %) of SWCNT-P4VP-Pt-POM in response to 0.5% of CH_4 in air (RH = 10 ± 5%). (*B*) Averaged conductance trace of SWCNT-P4VP-Pt-POM in response to three repeated 120-s exposures of 0.5% of CH_4 each in air. (*C*) Chemiresistive responses of SWCNT-P4VP-Pt-POM to 120-s exposures to various CH_4 concentrations in air (maroon), dry air (gray), or N_2 (blue) carrier gas. (*D*) Chemiresistive responses of SWCNT-P4VP-Pt-POM to 120-s exposures to various CH_4 concentrations in air. Shaded areas and error bars represent SDs (n = 4); all data were collected at room temperature.

that the Pt complex is likely immobilized by the substitution of the DMSO ligand by P4VP in SWCNT-P4VP-Pt (Fig. 2*B*).

To understand the speciation of the Pt complex in SWCNT-P4VP-Pt-POM following the anion exchange with $[H_5PV_2Mo_{10}O_{40}]$, the solution-state reactivity of the POM with the model complex [1-Py][SO_3OCH_3] was next examined. Addition of $[H_5PV_2Mo_{10}O_{40}]$ to a DMSO-d_6 solution containing [1-Py][SO_3OCH_3] initially resulted in anion exchange to furnish $[1\text{-Py}][H_4PV_2Mo_{10}O_{40}]$. However, monitoring the DMSO-d_6 solution of $[1\text{-Py}][H_4PV_2Mo_{10}O_{40}]$ by ^{1}H NMR spectroscopy over the course of 18 h at room temperature revealed that the polyoxometalate anion partially protonates the coordinated pyridine to yield an equilibrium mixture of products containing the starting $[1\text{-Py}][H_4PV_2Mo_{10}O_{40}]$ complex, as well as $[1\text{-DMSO}]^+$, and pyridinium (Fig. 4). These results indicate that the speciation of SWCNT-P4VP-Pt-POM is likely best described as containing protonated pyridyl groups, in addition to P4VP- and DMSO-ligated cationic platinum bipyrimidine complexes that are immobilized by P4VP coordination and electrostatic attraction to POM anions, respectively (Fig. 2*C*). A solid-state IR spectrum of the isolated equilibrium mixture containing $[1\text{-Py}][H_4PV_2Mo_{10}O_{40}]$ and $[1\text{-DMSO}][\text{Py-H}][H_3PV_2Mo_{10}O_{40}]$ exhibited diagnostic peaks that matched those observed for the SWCNT-P4VP-Pt-POM film, validating the relevance of the model system to the chemiresistor surface composition (*SI Appendix*, Fig. S16). Importantly, these model studies demonstrate that the known CH_4 oxidation precatalyst $[1\text{-DMSO}][H_4PV_2Mo_{10}O_{40}]$ is present on the chemiresistor surface and likely provides a facile entry point to CH_4 oxidation. Indeed, stirring a D_2O slurry of the isolated equilibrium mixture containing $[1\text{-Py}][H_4PV_2Mo_{10}O_{40}]$, $[1\text{-DMSO}]^+$, and pyridinium under an atmosphere of CH_4 furnished CH_3O(H/D) as observed by ^{1}H NMR spectroscopy (*SI Appendix*, Fig. S17).

Chemiresistor Selectivity Studies. Having examined the chemiresistive response of SWCNT-P4VP-Pt-POM to CH_4 and its origin, we next tested the selectivity and stability of our device. Accordingly, the response of SWCNT-P4VP-Pt-POM upon exposure to representative contaminants likely to be found in a CH_4 stream were tested. The results are shown in Fig. 5*A* and demonstrate that SWCNT-P4VP-Pt-POM exhibits mild selectivity for CH_4 over hydrocarbons such as n-hexane as well as benzene/toluene/o-xylene (BTX). These results are particularly surprising because, for a given concentration, higher boiling hydrocarbons partition to the sensor surface more effectively when compared to volatile CH_4. As a consequence, BTX and n-hexane typically give rise to significantly larger responses in sensors relying on traditional sensing mechanisms such as swelling (24, 25). While the mild selectivity observed for CH_4 appears to be a

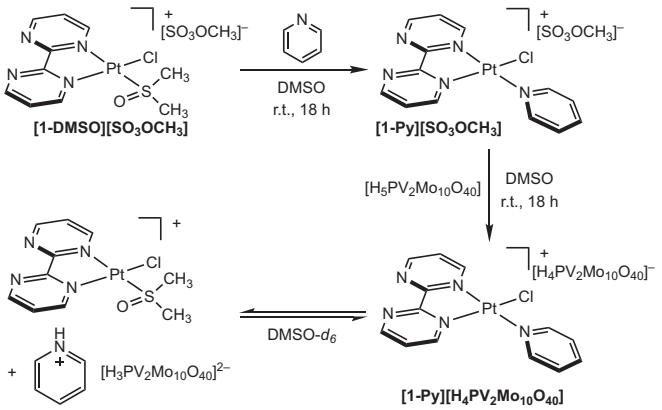

Fig. 4. Synthesis of [1-Py][SO_3OCH_3] and subsequent reaction with $[H_5PV_2Mo_{10}O_{40}]$.

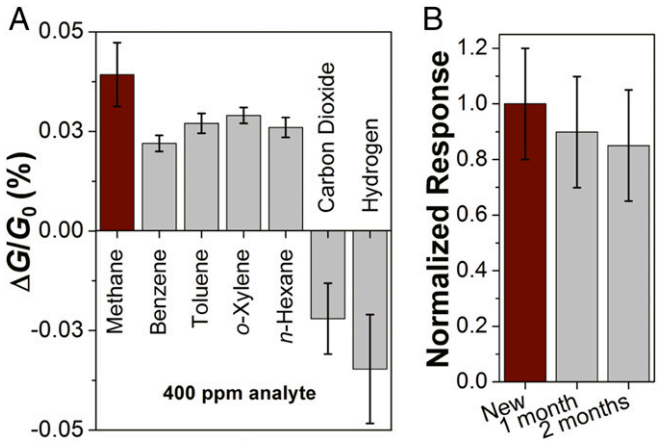

Fig. 5. Chemiresistor selectivity and stability studies. (*A*) Average device response (defined as change in conductance, $\Delta G/G_0$, %) of SWCNT-P4VP-Pt-POM toward 400 ppm of various interferants in air. (*B*) Normalized average response of freshly prepared and aged SWCNT-P4VP-Pt-POM devices toward 0.5% of CH_4 in air. Error bars represent SDs (n = 4); all data were collected at room temperature.

unique feature of SWCNT-P4VP-Pt-POM, the observation of a sensor response to *n*-hexane as well as BTX are qualitatively consistent with the proposed sensing mechanism, as Shilov-type oxidation precatalysts are expected to engage both aliphatic as well as aromatic hydrocarbons (50).

In addition to heavier hydrocarbons, the response of SWCNT-P4VP-Pt-POM to interferant gases commonly found in processed CH_4 streams was also examined. Specifically, SWCNT-P4VP-Pt-POM was found to exhibit selectivity for CH_4 over carbon dioxide (CO_2) as well as hydrogen (H_2). Upon exposure to these gases, a decrease in device conductance was observed that points to *n*-type doping, the opposite of the *p*-type sensor response to CH_4 (Fig. 5*A*). The observed reversal in response likely indicates a mechanistic pivot for the nonhydrocarbon analytes and provides a diagnostic detection handle for differentiating CH_4 from CO_2 and H_2 using SWCNT-P4VP-Pt-POM. Importantly, the device showed excellent stability over time with minimal loss of CH_4 response after storage on a laboratory bench for 2 mo, a consequence of its robust, air- and moisture-stable components (Fig. 5*B*).

Handheld Multimeter Sensing. To evaluate the potential utility of our sensor outside of a laboratory setting, we also tested the CH_4 sensing performance of SWCNT-P4VP-Pt-POM using a simple handheld multimeter. In this experiment, we connected the multimeter leads directly to the sensing chamber and monitored the resistance readout. Using a device that was previously stored on the laboratory benchtop for 2 mo, we observed a resistance change from 2.250 kΩ to 2.235 kΩ upon exposure to 5,000 ppm of CH_4 in air for 120 s at room temperature, corresponding to a 0.67% increase in device conductance (*SI Appendix*, Fig. S11). This result highlights that costly analytical equipment is not needed to obtain a diagnostic CH_4 response using SWCNT-P4VP-Pt-POM.

Conclusions. In summary, we developed a chemiresistive CH_4 sensor fabricated from SWCNT-P4VP composites incorporating a platinum-polyoxometalate-based CH_4 oxidation precatalyst. The chemiresistor operates at room temperature in air, offers ppm-level sensitivity for CH_4, as well as selectivity over heavier hydrocarbons and gases such as CO_2, and H_2. We also showed that the devices can be used in conjunction with a handheld multimeter, highlighting the potential of our method for the rapid, inexpensive, and portable detection of CH_4. The strategy presented herein should inspire further efforts to leverage molecular bond activation concepts for the detection of challenging analytes.

Data Availability. All study data are included in the article and *SI Appendix*.

ACKNOWLEDGMENTS. The authors gratefully acknowledge Eni S.p.A. for funding this research.

1. G. Myhre *et al*, "Anthropogenic and natural radiative forcing" in *Climate Change 2013: The Physical Science Basis. Contribution of Working Group I to the Fifth Assessment Report of the Intergovernmental Panel on Climate Change*, T. F. Stocker *et al*, Eds. (Cambridge University Press, Cambridge, UK, 2013), pp. 659–740.
2. M. G. Zabetakis, Flammability characteristics of combustible gases and vapors. *U.S. Bureau of Mines Bulletin* **627**, 1–121 (1965).
3. E. J. Dlugokencky, L. P. Steele, P. M. Lang, K. A. Masarie, The growth rate and distribution of atmospheric methane. *J. Geophys. Res.* **99**, 17021–17043 (1994).
4. J. Shemshad, S. M. Aminossadati, M. S. Kizil, A review of developments in near infrared methane detection based on tunable diode laser. *Sens. Actuators B Chem.* **171-172**, 77–92 (2012).
5. D. R. Caulton *et al*., Toward a better understanding and quantification of methane emissions from shale gas development. *Proc. Natl. Acad. Sci. U.S.A.* **111**, 6237–6242 (2014).
6. D. R. Caulton *et al*., Importance of superemitter natural gas well pads in the marcellus shale. *Environ. Sci. Technol.* **53**, 4747–4754 (2019).
7. T. Hong *et al*., State-of-the-art of methane sensing materials: A review and perspectives. *Trends Analyt. Chem.* **78**, 115820 (2020).
8. J. Kamieniak, E. P. Randviir, C. E. Banks, The latest developments in the analytical sensing of methane. *Trends Analyt. Chem.* **73**, 146–157 (2015).
9. N. S. Lawrence, Analytical detection methodologies for methane and related hydrocarbons. *Talanta* **69**, 385–392 (2006).
10. A. Baranov, D. Spirjakin, S. Akbari, A. Somov, Optimization of power consumption for gas sensor nodes: A survey. *Sens. Actuators A Phys.* **233**, 279–289 (2015).
11. H. Ma, E. Ding, W. Wang, Power reduction with enhanced sensitivity for pellistor methane sensor by improved thermal insulation packaging. *Sens. Actuators B Chem.* **187**, 221–226 (2013).
12. A. Dey, Semiconductor metal oxide gas sensors: A review. *Mater. Sci. Eng. B* **229**, 206–217 (2018).
13. D. Haridas, V. Gupta, Enhanced response characteristics of SnO_2 thin film based sensors loaded with Pd clusters for methane detection. *Sens. Actuators B Chem.* **166-167**, 156–164 (2012).
14. N. M. Vuong *et al*., Ni_2O_3-decorated SnO_2 particulate films for methane gas sensors. *Sens. Actuators B Chem.* **192**, 327–333 (2014).
15. G.-C. Liang *et al*., Photoacoustic trace detection of methane using compact solid-state lasers. *J. Phys. Chem. A* **104**, 10179–10183 (2000).
16. Z. Wang *et al*., Methane-oxygen electrochemical coupling in an ionic liquid: A robust sensor for simultaneous quantification. *Analyst (Lond.)* **139**, 5140–5147 (2014).
17. T. Otagawa, S. Zaromb, J. R. Stetter, Electrochemical oxidation of methane in nonaqueous electrolytes at room temperature: Application to gas sensors. *J. Electrochem. Soc.* **132**, 2951–2957 (1985).
18. J. A. Garcia, L. M. Dorojkine, A. Mandelis, J. S. Wallace, Thermophysical response of a solid-state thermal-wave pyroelectric-film sensor to natural gas and methane. *Int. J. Hydrogen Energy* **21**, 761–764 (1996).
19. T. M. Swager, Sensor technologies empowered by materials and molecular innovations. *Angew. Chem. Int. Ed. Engl.* **57**, 4248–4257 (2018).
20. D. R. Kauffman, A. Star, Carbon nanotube gas and vapor sensors. *Angew. Chem. Int. Ed. Engl.* **47**, 6550–6570 (2008).
21. V. Schroeder, S. Savagatrup, M. He, S. Lin, T. M. Swager, Carbon nanotube chemical sensors. *Chem. Rev.* **119**, 599–663 (2019).
22. A. M. Rao, P. C. Eklund, S. Bandow, A. Thess, R. E. Smalley, Evidence for charge transfer in doped carbon nanotube bundles from Raman scattering. *Nature* **388**, 257–259 (1997).
23. J. Kong *et al*., Nanotube molecular wires as chemical sensors. *Science* **287**, 622–625 (2000).
24. P. C. Jurs, G. A. Bakken, H. E. McClelland, Computational methods for the analysis of chemical sensor array data from volatile analytes. *Chem. Rev.* **100**, 2649–2678 (2000).
25. C. M. Hangarter, N. Chartuprayoon, S. C. Hernández, Y. Choa, N. V. Myung, Hybridized conducting polymer chemiresistive nano-sensors. *Nano Today* **8**, 39–55 (2013).
26. X. Tang *et al*., Carbon nanotube DNA sensor and sensing mechanism. *Nano Lett.* **6**, 1632–1636 (2006).
27. J. Wang, C. Timchalk, Y. Lin, Carbon nanotube-based electrochemical sensor for assay of salivary cholinesterase enzyme activity: An exposure biomarker of organophosphate pesticides and nerve agents. *Environ. Sci. Technol.* **42**, 2688–2693 (2008).
28. Y. Weizmann, D. M. Chenoweth, T. M. Swager, DNA-CNT nanowire networks for DNA detection. *J. Am. Chem. Soc.* **133**, 3238–3241 (2011).

29. B. Esser, J. M. Schnorr, T. M. Swager, Selective detection of ethylene gas using carbon nanotube-based devices: Utility in determination of fruit ripeness. *Angew. Chem. Int. Ed. Engl.* **51**, 5752–5756 (2012).
30. A. Star, V. Joshi, S. Skarupo, D. Thomas, J.-C. P. Gabriel, Gas sensor array based on metal-decorated carbon nanotubes. *J. Phys. Chem. B* **110**, 21014–21020 (2006).
31. Y. Lu *et al*., Room temperature methane detection using palladium loaded single-walled carbon nanotube sensors. *Chem. Phys. Lett.* **391**, 344–348 (2004).
32. M. T. Humayun *et al*., Novel chemoresistive CH_4 sensor with 10 ppm sensitivity based on multiwalled carbon nanotubes functionalized with SnO_2 nanocrystals. *J. Vac. Sci. Technol. A* **34**, 01A131-1–01A131-7 (2016).
33. M. T. Humayun *et al*., ZnO functionalization of multiwalled carbon nanotubes for methane sensing at single parts per million concentration levels. *J. Vac. Sci. Technol. B* **33**, 06FF01-1–06FF01-7 (2015).
34. V. Schroeder, T. M. Swager, Translating catalysis to chemiresistive sensing. *J. Am. Chem. Soc.* **140**, 10721–10725 (2018).
35. D. Fong, S.-X. Luo, R. S. Andre, T. M. Swager, Trace ethylene sensing via wacker oxidation. *ACS Cent. Sci.* **6**, 507–512 (2020).
36. I. Bar-Nahum, A. M. Khenkin, R. Neumann, Mild, aqueous, aerobic, catalytic oxidation of methane to methanol and acetaldehyde catalyzed by a supported bipyrimidinylplatinum-polyoxometalate hybrid compound. *J. Am. Chem. Soc.* **126**, 10236–10237 (2004).
37. J. M. Villalobos, A. J. Hickman, M. S. Sanford, Platinum(II) complexes containing quaternized nitrogen ligands: Synthesis, stability, and evaluation as catalysts for methane and benzene H/D exchange. *Organometallics* **29**, 257–262 (2010).
38. J. H. Rouse, Polymer-assisted dispersion of single-walled carbon nanotubes in alcohols and applicability toward carbon nanotube/sol-gel composite formation. *Langmuir* **21**, 1055–1061 (2005).
39. B. Yoon, S. F. Liu, T. M. Swager, Surface-anchored poly(4-vinylpyridine)–single-walled carbon nanotube–metal composites for gas detection. *Chem. Mater.* **28**, 5916–5924 (2016).
40. Sigma-Aldrich, Data from Sigma-Aldrich FTIR documentation for "methyl sulfate sodium salt". https://www.sigmaaldrich.com/spectra/rair/RAIR008269.PDF. Accessed 1 October 2020.
41. B. Yoon, S.-J. Choi, T. M. Swager, G. F. Walsh, Switchable single-walled carbon nanotube-polymer composites for CO_2 sensing. *ACS Appl. Mater. Interfaces* **10**, 33373–33379 (2018).
42. J. Li *et al*, Carbon nanotube sensors for gas and organic vapor detection. *Nano Lett.* **3**, 929–933 (2003).
43. J. A. Labinger, J. E. Bercaw, The role of higher oxidation state species in platinum-mediated C–H bond activation and functionalization. *Top. Organomet. Chem.* **35**, 29–60 (2011).
44. N. J. Gunsalus *et al*., Homogeneous functionalization of methane. *Chem. Rev.* **117**, 8521–8573 (2017).
45. P. G. Collins, K. Bradley, M. Ishigami, A. Zettl, Extreme oxygen sensitivity of electronic properties of carbon nanotubes. *Science* **287**, 1801–1804 (2000).
46. D. Kang, N. Park, J. Ko, E. Bae, W. Park, Oxygen-induced p-type doping of a long individual single-walled carbon nanotube. *Nanotechnology* **16**, 1048–1052 (2005).
47. R. Neumann, Polyoxometalate complexes in organic oxidation chemistry. *Prog. Inorg. Chem.* **47**, 317–370 (1998).
48. R. Neumann, Activation of molecular oxygen, polyoxometalates, and liquid-phase catalytic oxidation. *Inorg. Chem.* **49**, 3594–3601 (2010).
49. G. A. Tsigdinos, C. J. Hallada, Molybdovanadophosphoric acids and their salts. I. Investigation of methods of preparation and characterization. *Inorg. Chem.* **7**, 437–441 (1968).
50. M. Lersch, M. Tilset, Mechanistic aspects of C-H activation by Pt complexes. *Chem. Rev.* **105**, 2471–2526 (2005).